Environmental Effects on Metallic Corrosion Products Formed in Short-Term Atmospheric Exposures

D. R. Flinn, S. D. Cramer, J. P. Carter, D. M. Hurwitz, and P. J. Linstrom

Bureau of Mines, U.S. Department of the Interior, Avondale, MD 20782-3393

Downloaded via CENTERS DISEASE CONTROL & PRVNTN on November 12, 2021 at 17:15:22 (UTC).
See https://pubs.acs.org/sharingguidelines for options on how to legitimately share published articles.

The Bureau of Mines has measured short- and long-term atmospheric corrosion damage on five metals and two metal-coated steel products at four sites in the east and northeast United States as part of the National Acid Precipitation Assessment Program to evaluate the effects of acid deposition on materials. The composition of the corrosion product on carbon steel, weathering steel, copper, zinc, and galvanized steel is relatively unchanged in 1- and 3-month exposures over a wide variety of environmental conditions. Spalling and runoff losses are observed on all metals. Massive reorganization of the corrosion film by a mechanism of cyclic dissolution and precipitation was observed on carbon steel, Cor-Ten A, zinc, and galvanized steel. Loss of corrosion product from zinc in runoff was a function of both dissolution in rain water and neutralization by hydrogen ion loading, with dissolution contributing the greater portion of the loss.

The corrosion of metallic materials in the atmosphere has been studied extensively (1). The majority of the work in this area has been to determine the performance of materials and to evaluate mitigation techniques in environments of interest. With only a few exceptions (see for example references 2, 3), attempts have not been made in studies conducted in the United States to fully characterize the environment and to determine the relationships between components of the environment and the performance of the material of interest (see reference 4 for a recent assessment of this area). Adherent corrosion products are often characterized, but no attempts have been made, except in laboratory studies (5), to quantitatively relate the corrosion film chemistry to environmental parameters.

In 1981, a field study was initiated by the Bureau of Mines to determine the effects of the environment, including acid deposition, on the corrosion of a number of commonly used metallic materials of construction. This study, which is fully described in a recent paper (6), is being conducted at field sites where continuous air

This chapter not subject to U.S. copyright.
Published 1986, American Chemical Society

quality, rain chemistry, and meteorology measurements are being made. Of equal importance, the corrosion products are characterized by both wet chemical and instrumental methods in order to provide additional information regarding environmental effects on the materials. In this paper, the results of the corrosion product characterizations for short-term (generally 1 year or less) exposures are described.

Experimental

The field study is being conducted at five sites: Research Triangle Park, NC; Washington, DC; Chester, NJ; Newcomb, NY; and a recently added site at Steubenville, OH. These sites encompass the range of gaseous pollutant levels and meteorology variables typically observed in most rural, urban, and suburban locations in the United States. Hydrogen ion loading in the rainfall varies by a factor of 2 between the four original sites, and annual average rainfall pH ranges from 4.18 to 4.41.

The metals exposed in the program are 1010 carbon steel, Cor-Ten A[1] weathering steel, 3003-H14 aluminum, 110 copper, rolled zinc (alloy 191), G-90 galvanized steel, and Galvalume (a 55Al-45Zn coating on steel). Weight-loss samples, 4 by 6 inches, are installed (in triplicate) and removed following preselected exposure periods of 1 month, 3 months, 1 year, and 3 years; the 3-month and 1-year exposures are installed every 3 months, with the winter season defined as December through February. The sample exposure racks are inclined at 30° to the horizon and face south. After the exposed samples are weighed, the corrosion product is chemically removed from the weight-loss samples, and these stripping solutions are analyzed by standard chemical techniques (7). The cleaned samples are weighed again to determine metal loss during exposure. Smaller, 1 by 1.75 inch, samples ("microanalysis samples") are exposed concurrently with the larger samples.

The microanalysis samples are used in studies of the corrosion film by a number of instrumental techniques. X-ray diffraction (XRD) was performed on a Phillips X-ray diffraction unit at 40 KV using CuKα radiation. Samples were examined on an ISI scanning electron microscope (SEM) using backscattered electrons. Elemental depth profiles for the corrosion films were measured by a combination of ion scattering spectroscopy (ISS) and ion etching with $^{3}He^{+}$ at a rate of 0.3 to 0.5 nm per minute. Chemical information from the corrosion film surfaces was obtained with a Surface Science Laboratory SSX-100 X-ray photoelectron spectrometer (XPS) using an AlKα monochromatic X-ray source. Thermogravimetric analysis (TGA) was conducted using a Cahn RH vacuum electrobalance system and a Cahn Mark II time derivative computer to determine the amount of water in the corrosion films and the presence of compounds that may decompose at temperatures up to about 600° C. TGA was done in an argon atmosphere.

For complete description of the site environments, materials studied, and experimental procedures, see reference 6. Complete

computer files of the air quality and meteorology data are being prepared so that it will soon be possible to evaluate correlations between these data and the metallic corrosion rates. With the exception of Steubenville, OH, more than 2 years of corrosion rate data (25 one-month exposure periods, 11 three-month periods, and 7 year-long exposures) have been measured at each site.

Results and Discussion

Table I shows the average corrosion rates observed for Cor-Ten A, zinc, and copper in 1-month, 3-month, and 1-year exposures. The corrosion rates for copper and zinc were lowest at the Washington, DC, site, while the Cor-Ten A corrosion rate was lowest at the New York site. The corrosion rates for galvanized steel and for Galvalume were less than 1 μm/y in exposures up to 1 year. The corrosion rate for aluminum, as expected, was low (less than 0.1 μm/y).

Table I. Average corrosion rates at four field sites

Metal	Exposure[1] Months	Corrosion Rate, μm/y			
		NC	DC	NJ	NY
Cor-Ten A	1	33.8	50.7	43.4	18.6
	3	27.1	36.3	34.5	14.7
	12	16.1	15.1	20.1	10.6
191 Zinc	1	6.5	1.0	3.5	4.6
	3	2.6	0.9	2.0	2.4
	12	1.4	1.1	1.4	1.0
110 Copper	1	6.2	1.9	5.4	5.8
	3	4.3	1.4	3.6	3.8
	12	2.4	1.1	2.2	2.1

[1]One-month exposures for period May 1982 through May 1984; 3- and 12-month exposures begun in period March 1982-December 1983.

In a general way, the growth of a corrosion film on a metal can be viewed schematically as a process with three distinct steps. The first is the reaction of metal A with environmental species B

$$A + B \rightarrow AB \tag{1}$$

The second step is the interaction of this corrosion product with environmental factors such as the weather, gaseous pollutants, and wet and dry deposition to produce, while conserving metal in the film, a modified or weathered corrosion product AB*

$$AB + \text{environment} \rightarrow AB^* \tag{2}$$

The third involves the loss of mass from the corrosion product through mechanical and chemical processes

$$AB^* + \text{environment} = AB^{**} + R_L + S_L \tag{3}$$

where R_L represents the runoff losses produced by the dissolution and removal of corrosion product in precipitation, and S_L represents the spalling losses caused by thermal and volume distortion stresses. In a well-developed corrosion film, all three steps may be occurring at the same time.

If m_A is the mass of A lost due to corrosion, S_L and R_L are the mass of A lost from m_A in spalling and runoff, and $m_{AB^{**}}$ is the mass of weathered corrosion product retained on the metal in Equation 3, then a mass balance for the corrosion film yields:

$$m_{AB^{**}} = (m_A - R_L - S_L)\left[\sum_{i=1}^{N} X_i \left(\frac{M_i}{M_A}\right)\right] \tag{4}$$

where X_i is the fraction of A in the i-th constituent of $m_{AB^{**}}$, compared to the total mass of A retained in $m_{AB^{**}}$. M_A and M_i are the molecular weight of A and the i-th constituent, respectively, N is the number of constituents present in AB**, and

$$\sum_{i=1}^{N} X_i = 1 \tag{5}$$

For some materials, runoff and spalling losses are negligible in short-term exposures, e.g., $R_L = S_L = 0$, so that m_A replaces $(m_A - R_L - S_L)$ in Equation 4. If, furthermore, the system of oxides, hydroxides, etc., which comprise the corrosion product are thermodynamically stable, i.e., relatively insensitive to changes in the environment so that the composition does not vary greatly, a plot of $m_{AB^{**}}$ as a function of m_A, using the gravimetrically determined film weight and weight-loss data, should yield a straight line with slope

$$b = m_{AB^{**}}/m_A = \sum_{i=1}^{N} X_i \left(\frac{M_i}{M_A}\right) \tag{6}$$

such as that shown in Figure 1 for Cor-Ten A. The concentration, X_i^*, of the i-th constituent in the corrosion product expressed as a fraction of $m_{AB^{**}}$ is then

$$X_i^* = \frac{X_i m_A}{m_{AB^{**}}}\left(\frac{M_i}{M_A}\right) = \left(\frac{X_i}{b}\right)\left(\frac{M_i}{M_A}\right) \tag{7}$$

Data presented as in Figure 1 has the advantage of accentuating differences due to spalling and runoff losses. These differences result in points which lie below the line describing the short-term data.

In cases where runoff or spalling losses are significant, $(m_A - R_L - S_L)$ must be estimated from an analysis of the corrosion product retained on the corroding metal. This was done by wet chemical analysis of the stripping solutions that contain the corrosion product removed from exposed samples. Again, if the corrosion product is thermodynamically stable for a wide range of environmental

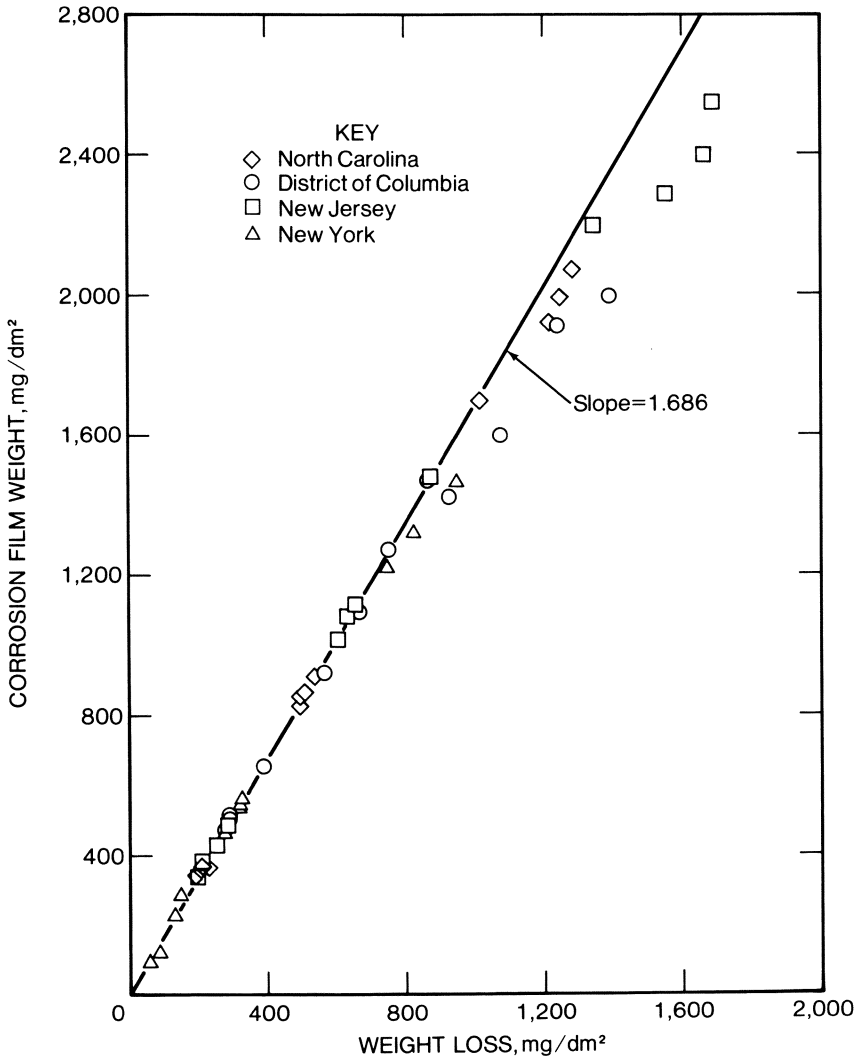

Figure 1. Mass of corrosion product retained on Cor-Ten A weight-loss panels in exposures of 1, 3, and 12 months at 4 sites. Exposures were initiated in period May 1982 - May 1983.

conditions, Equation 4 shows that a plot of m_{AB**} as function of $(m_A-R_L-S_L)$ should yield a straight line with a slope

$$b = \frac{m_{AB**}}{(m_A-R_L-S_L)} \tag{8}$$

With this approach, spalling and runoff losses do not affect the computation of the slope. On the other hand, the precision of the wet chemical measurements is lower than for the gravimetric measurements and slopes computed by Equation 8 are not as well defined as those from Equation 6. In the limit when $S_L=R_L=0$, these two approaches to computing the slopes give similar results.

Experimental estimates of b are given in Table II. Except for galvanized steel, these values were calculated using gravimetric results and Equation 6. For galvanized steel, b was calculated from wet chemical results for the amount of zinc in the corrosion film, i.e., $(m_A-R_L-S_L)$ and Equation 8. The number of data points, N, used in the computation are also given to show that the slopes are based on a large data set. Experimental values of the relative uncertainty in b, i.e., $\Delta b/b$, are given in Table II, column 5, as $2tS/b$, where S is the standard error in the estimate of b, and t is the measure of the dispersion about b, at a given confidence level. One- and 3-month exposure gravimetric data were used to compute b for Cor-Ten A and carbon steel since 1-year data showed evidence of spalling losses (confirmed by SEM examination) and to a lesser extent runoff losses. One- and 3-month gravimetric data were also used for copper. The zinc and galvanized data showed considerable scatter due to runoff losses. No spalling of these materials was observed using SEM examination of their surfaces. The 1- and 3-month exposure zinc gravimetric data define an upper limit to the amount of corrosion film retained on the zinc and were used to compute the slope b. On the other hand, the galvanized steel data had much more scatter than the zinc data and defining the limiting slope was more difficult. As noted above, this was overcome by using the wet chemical estimate for $(m_A-R_L-S_L)$ in Equation 8.

Table II. Relative sensitivity factor and experimental slopes

Metal	$(1/b)\partial b/\partial x$	Constituents	b	$2tS/b$[1]	N
Cor-Ten A	1	FeOOH or Fe_2O_3, H_2O	1.686	0.005	420
1010 Carbon Steel	1	FeOOH or Fe_2O_3, H_2O	1.677	0.009	425
191 Zinc	0.2	$Zn(OH)_2$, $ZnCO_3$	1.645	0.014	280
Galvanized Steel	0.4	ZnO, $ZnCO_3$	1.512	0.030	136
110 Copper	0.1	CuO, Cu_2O	1.115	0.007	429

[1]S evaluated at 99 pct confidence level for all metals except galvanized steel; galvanized steel evaluated at 90 pct confidence level.

The sensitivity of the slope b to changes in the composition of the corrosion film is characterized by the relative sensitivity factor, $(1/b)\partial b/\partial x$. Values of this factor are given in Table II for the case where the corrosion film consists of the 2 major constituents shown in column 3. Cor-Ten A and 1010 carbon steel had the highest sensitivity factor; a 1 pct change in composition would result in a 1 pct change in slope. Copper had the lowest sensitivity factor and a 1 pct change in composition would result in only a 0.1 pct change in slope. Comparing values of the relative uncertainty in b, column 5, with the sensitivity factors suggests that the composition of most of the corrosion films in short exposures is independent of environmental influences. In fact, using the 2-constituent corrosion film model, the experimental slopes define the amount of each constituent in the corrosion product to within several weight percent. Of course, the corrosion films on these materials are more complicated than the 2-constituent model. Nevertheless, these results indicate that the composition of the corrosion films is quite stable and that, regardless of site-to-site differences in the important environmental factors, the relative amounts of each constituent are fairly constant. The major influence of the environmental factors then is not to alter the thermodynamic stability of the corrosion products but to influence the kinetics of the rate limiting corrosion reaction.

Consider now Equation 3 describing losses of corrosion product. Assuming that spalling does not occur, evidently true for most materials in this study except Cor-Ten A and carbon steel, and that dry deposition effects can be neglected, the principal effects leading to loss of corrosion product in runoff are: (1) dissolution of the corrosion product in rainwater; and (2) reaction of corrosion product with hydrogen ion in the rain to form a more soluble species. Let the flux of hydrogen ion, i.e., the hydrogen ion load, to the skyward side of the weight loss panels be x (in mg H^+/m^2) and the flux of precipitation be y (in L H_2O/m^2). The loss of metal A from the corrosion product AB* to runoff is R_L (in mg A/dm^2). For simplicity, assume that the AB* is a single compound. Let H^+ react with this product according to

$$AB^* + nH^+ \rightarrow A^{n+} + H_nB^* \tag{9}$$

The amount of AB consumed in runoff due to this reaction is (xM_A/nM_H), where M_H and M_A are the molecular weights of H and A, respectively. In addition, the amount of A dissolved as AB* in H_2O is $fS_{AB*}y(M_A/M_{AB*})$, where S_{AB*} is the solubility of AB* in water (in mg AB*/L), M_{AB*} is the molecular weight of AB*, and f is the fraction of saturation that is achieved. This fraction is likely to be below 1.0 since the residence time for precipitation on the inclined surface of the panels is short. Combining terms, rationalizing units, and correcting areas for the incline of the panel leads to:

$$R_L = \frac{\cos 30^\circ}{200}\left[fS_{AB*}\, y\left(\frac{M_A}{M_{AB*}}\right) + \left(\frac{M_A}{M_H}\right)\frac{x}{n}\right] \tag{10}$$

This equation includes a factor of 2 because runoff is assumed to occur only from the skyward side but m_A, m_{AB**}, S_L, and R_L are computed based on the total sample surface area (skyward and

groundward). This equation has the same form as that used to interpret wet deposition damage to stone (4, 8, 9). It predicts that total runoff losses involve contributions from both solubility and hydrogen ion effects.

Carbon Steel and Cor-Ten A Steel. The corrosion rates for Cor-Ten A steel at the four sites are shown in Table I. Corrosion rates for carbon steel at the North Carolina, District of Columbia, and New Jersey sites are lower than those for Cor-ten A during 1-month exposures, equal to Cor-ten A during 3-month exposures, and higher than Cor-ten A for 1-year exposures. Corrosion rates for carbon steel at the New York site are lower than Cor-ten A during the 1- and 3-month exposures and equal to Cor-ten A after 1 year of exposure. These results indicate, relative to carbon steel, that Cor-ten A must corrode a definite amount before producing a corrosion film of sufficient thickness to exhibit protective properties.

The formation and composition of atmospheric rust films on carbon steel and weathering steels has been discussed extensively in the literature (10-22). In general, the rust which forms on steels can be viewed as a 2-layer structure generated by an electrochemical corrosion cycle which involves the oxidation of metal and reduction of oxide corrosion products in the inner layer and oxidation of reduced corrosion products in the outer layer. The corrosion film is basic in nature and comprised essentially of a series of oxides and oxyhydroxides representing partially dehydrated forms of ferric hydroxide. The corrosion product in the outer layer dissolves during wet periods and reprecipitates as amorphous $FeO_x(OH)_{3-2x}$ upon drying. The differences in the corrosion of carbon steel and weathering steel have been attributed to the enrichment of alloying elements in the inner rust layer which (1) favors the formation of amorphous subtances which strengthen the rust coating, (2) increases the amount of water found in the corrosion film and slows drying to produce a more compact film, and (3) decreases the formation of intermediate substances that can form crystalline magnetite and improve the conductivity of the rust coating.

A plot of metal weight loss (m_A) for 1-, 3-, and 12-month exposures of Cor-Ten A at the 4 sites versus film weight, m_{AB**}, is shown in Figure 1. The slope of the line for 1- and 3-month data was 1.686. The narrow confidence limits for the slope, Table II, indicate that the corrosion film composition is similar at all sites for short-term exposures. This means that the thermodynamically favored corrosion products are the same regardless of site. Carbon steel gave similar results. Deviations from the straight line at higher weight-loss values correspond to 1-year data. Based on an SEM examination of the corrosion films, much of this loss is the result of spalling. Rust staining of the corrosion test racks indicates that runoff losses also occur. The slope of 1.686 for Cor-Ten A suggests that the corrosion film is largely FeOOH and hydrated Fe_2O_3, Table III. It is unlikely that FeO, Fe_3O_4, or Fe_2O_3 is present in large amounts as these products would bring the slope down significantly. Conversely, $Fe(OH)_3$ and $FeSO_4$ would raise it considerably. Carbon steel gave a similar slope and, at least in short-term exposures, the chemistry of the corrosion film on carbon steel and Cor-Ten A with respect to the major constituents apppears the same. If the corrosion film is assumed to be FeOOH, the computed

Table III. Corrosion film mass balance results from wet chemical and gravimetric estimates of metal retained in corrosion film

Metal	b Confidence Interval	Major Constituents		Comment
		Likely	Not Likely	
Cor-Ten A	1.68-1.69*	FeOOH $Fe_2O_3 \cdot nH_2O$	FeO Fe_3O_4 Fe_2O_3 $FeSO_4$ $Fe(OH)_3$	Contains 5 wt pct water of hydration
1010 Carbon Steel	1.67-1.68*	Same as Cor-Ten A		Same as Cor-Ten A
191 Zinc	1.633-1.657*	$ZnCO_3$ $Zn(OH)_2$	ZnO $ZnSO_4$ ZnS $ZnS \cdot H_2O$	Corrosion film 30 pct $ZnCO_3$ and 70 pct $Zn(OH)_2$ in short exposures
	1.617-1.945**	$ZnCO_3$ $Zn(OH)_2$		Corrosion film at 3 sites 65 wt pct $ZnCO_3$ and 35 wt pct $Zn(OH)_2$
		$ZnCO_3$ $Zn(OH)_2$ ZnO		DC site (b=1.436)
Galvanized Steel	1.156-1.200*	ZnO	$Zn(OH)_2$ $ZnCO_3$ $ZnSO_4$ ZnS $ZnS \cdot H_2O$	Low b for DC site
	1.489-1.535**	$ZnCO_3$ $Zn(OH)_2$ ZnO		
110 Copper	1.111-1.119*	Cu_2O CuO	Cu_2S CuS $CuSO_4$ $CuSO_4 \cdot 3Cu(OH)_2$ $Cu(OH)_2$ Cu_2CO_3 $CuCO_3 \cdot Cu(OH)_2$ $2CuCO_3 \cdot Cu(OH)_2$ $CuCl_2 \cdot 3Cu(OH)_2$	Low b for DC site. One-month DC data agrees with other sites; 3- and 12-month data fall below curve
	1.047-1.225**	Cu_2O CuO		DC data higher than other sites corresponding to 60 wt pct CuO and 40 wt pct Cu_2O

*Metal loss determined gravimetrically; 99 pct confidence level.
*Metal loss determined from wet chemical analysis of corrosion product 90 pct confidence level.

slopes would suggest that there is approximately 5 wt pct water present in the film.

The results from TGA, Table IV, indicate that the corrosion film on Cor-Ten A contains from 30 to 70 wt pct FeOOH. The

Table IV. Thermogravimetric analysis (TGA) of corrosion film on microanalysis samples

Metal	Major Constituents: Likely	Major Constituents: Not Likely	Description	Mass Balance Results
Cor-Ten A	FeOOH H_2O	$FeSO_4 \cdot H_2O$	Weight loss during bake-out, <70° C	4-12 wt pct, "free" H_2O
			Weight loss from 110°-160°C	1.7-4.4 wt pct water of hydration
			Large weight loss from 160°-260° C, e.g., "goethite terrace"	30-70 wt pct FeOOH
191 Zinc	$ZnCO_3$	$ZnSO_4 \cdot H_2O$ $Zn(OH)_2$	Small weight loss from 110° C to 150°-200° C	$Zn(OH)_2$ decomposition
			Large weight loss from 200°-250° C	40-100 wt pct $ZnCO_3$
110 Copper	—	$CuCO_3$ $CuCl_2 \cdot 2H_2O$ $CuSO_4$ CuS $CuCl_2 \cdot Cu(OH)_2$	Weight loss builds at small but steady rate from 110°-350° C	—

decomposition at 160°-260° C clearly matched the decomposition of goethite reported in the literature (23). There is 4 to 12 pct loosely bound water absorbed in the film, and 1.7 to 4.4 pct water more tightly bound as waters of hydration presumably as $Fe_2O_3 \cdot n\ H_2O$ or the amorphous iron oxyhydroxide. The only crystalline phase identified in the corrosion film was goethite, Table V. After TGA analysis, XRD analysis showed both magnetite and hematite present. This would indicate that decomposition of the corrosion film to Fe_3O_4, the expected final thermal decomposition product (24), is incomplete.

XPS analysis of the corrosion film on Cor-Ten A, Table VI, gives results similar to those obtained by corrosion film mass balance, TGA, and XRD. The principal film constituents in the outer 10 nm of the film are Fe_2O_3 and FeOOH, with there being somewhat more iron present as Fe_2O_3 than FeOOH. This would be expected in a film that dehydrates. However, if this is true, then the 2:1 atomic ratio of oxygen to iron indicates that even the outermost surface of the film contains substantial water. ISS depth profiles for the

Table V. X-ray diffraction analysis of corrosion film on microanalysis samples

Metal	Phases Present	
	3-year Exposure, Avondale, MD	After TGA
Cor-Ten A	Goethite (FeOOH)	Magnetite (Fe_3O_4) Hematite (Fe_2O_3)
1010 Carbon Steel	Goethite (FeOOH)	(1)
191 Zinc	Unknown phases	Zincite (ZnO)
110 Copper	Cuprite (Cu_2O)	Cuprite (Cu_2O)

(1) Not determined.

corrosion films on Cor-Ten A, Table VII, show sulfur (or Cl) present only at the surface, with concentrations dropping to zero in the first nm. Normalizing the data to Fe_2O_3 for the layer at 1-5 nm in depth, the corrosion film is rich in iron at the surface (0-5 nm), probably due to more extensive drying of the film. At depths greater than 15 nm, the film contains relatively more oxygen, corresponding to a compound such as FeOOH.

SEM examination of the corrosion films on Cor-Ten A and carbon steel from exposures of 1, 12, and 36 months showed massive reorganization of the corrosion product. In short-term exposures the corrosion film on carbon steel and Cor-Ten A is characterized by mounds of corrosion product, Figure 2A, produced by intense localized corrosion cells which lie beneath them. The displacement of this corrosion product outward, away from the metal-film interface, can cause severe fracturing of the corrosion film and give moisture easy access to the inner layer and the corroding surface. Superimposed on this general structure are 3 features which suggest the massive reorganization just noted. First, in longer exposures the mounds become an increasingly less distinct feature of the corroding surface. Their tops are flattened and the large space which had existed earlier between them is filled. Secondly, there is little evidence of healed cracks in the corrosion film, although there are numerous fresh cracks and the well-defined features of these cracks could not survive even moderate solution alteration of the surface. These cracks were also observed by light microscopy on samples which had not been exposed to the vacuum of the SEM. Third, there is abundant evidence of relocation by precipitation of large amounts of corrosion film. Figures 2B and 2C show just one such example. A reef-like feature in the top right corner of 2B is spreading laterally from its attachment to a mound as new material precipitated along its edges. In doing so, it is spreading outward over material which is in the "valley" between mounds, Figure 2C, and evidently will fill in this space. This is one mechanism whereby the mounds coalesce, as is occurring in the lower left quarter of Figure 2B, to

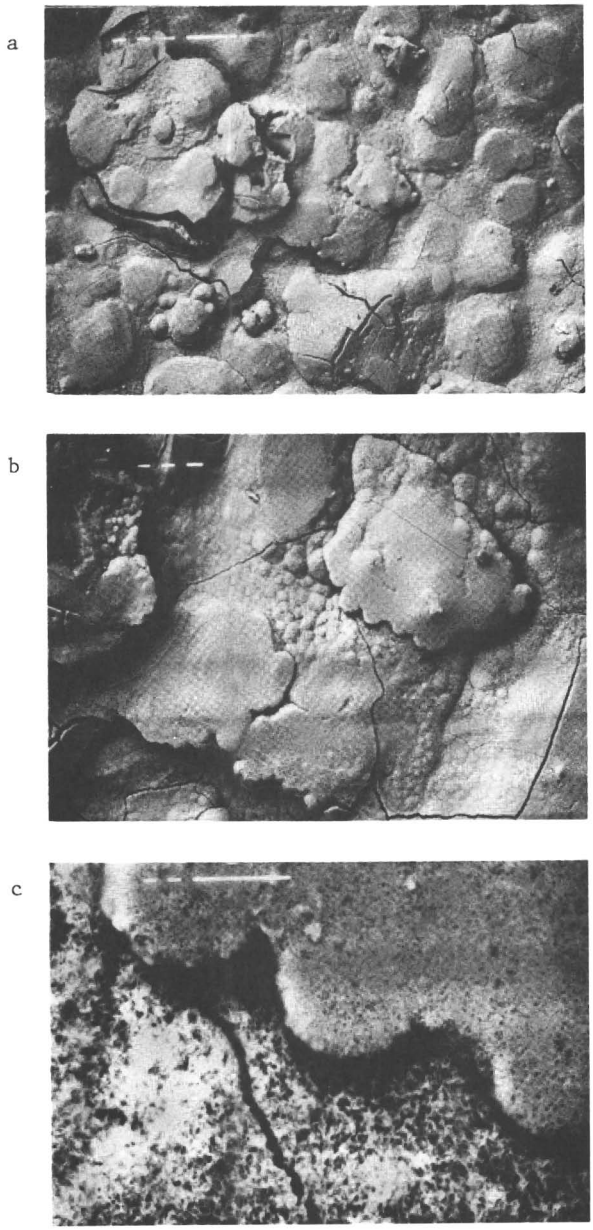

Figure 2. Groundward side of Cor-Ten A microsample E231 exposed 1 year at NC site showing dissolution and precipitation features. Magnifications: (a) 80X; (b) 240X; (c) 1600X.

Table VI. X-ray photoelectron spectroscopic analysis of corrosion film on microanalysis samples

Metal/Exposure	XPS Peak	Observation[1]
Cor-Ten A	$C1S_{1/2}$	C-C, C-H: major C-O, C=O: minor
	$O1S_{1/2}$	Fe_2O_3: major hydroxide [FeOOH], water: major C-O,C=O: minor O(as FeOOH)>O(as Fe_2O_3)
	$Fe2P_{3/2}$	Fe_2O_3: major FeOOH: major Fe(as FeOOH)<Fe(as Fe_2O_3) Note: O/Fe~2
Galvanized Steel	$C1S_{1/2}$	C-C, C-H: major CO_3: major
	$O1S_{1/2}$	hydroxide [$Zn(OH)_2$], water: major carbonate [$ZnCO_3$]: major oxide [Cr_2O_3 or CrO_3]: minor O(as $Zn(OH)_2$)> O(as $ZnCO_3$)
	$Zn2P_{3/2}$	2 peaks [$Zn(OH)_2$ and $ZnCO_3$]
	$Pb4f_{7/2}$	1 peak [PbO or Pb_3O_4]
	$Cr2P_{3/2}$	$\left.\begin{matrix}Cr_2O_3\\CrO_3\end{matrix}\right\}$ $Cr^{3+} \lesssim 6\ Cr^{6+}$

[1]Phases in brackets indicate probable identities of peaks.

Table VII. Ion scattering spectroscopic analysis of corrosion films on microanalysis samples

Metal	Distance From Outer Surface, nm	Description
Cor-Ten A	0-0.2	2-10 a/o Cl/S O rich layer (O/Fe>>1)
	0.2-1	1 a/o Cl/S Fe rich layer (O/Fe ~ 1)
	1-5	Fe_2O_3[1]
	>15	FeOOH (O/Fe~2.2) O a/o Cl/S
Zinc	0-1	10-55 a/o Cl/S ZnO
	1-15	0.5-5 a/o Cl/S ZnO, with 2-4 a/o excess Zn
	>15	O>Zn, composition shifting towards carbonate or hydroxide
Galvanized Steel	0-1	3-13 a/o Cr .2-2 a/o Al 16-29 a/o Zn 55-80 a/o O
	>1	ZnO 9-13 a/o Cr 2-7 a/o Al
Copper	0-0.3	3-8 a/o Cl/S 30-85 a/o Cu 10-62 a/o O
	0.3-2	CuO[1] 1-3 a/o Cl/S
	>2	Cu rich phase (Cu/O~1.6)

[1]Data normalized to this value for computational purposes.

give the smooth flat surface characteristic of the corrosion film formed in long exposures. For such a reef-like feature to grow, the "valley" or depressed area between mounds must be filled with a concentrated solution of dissolved rust. This of course could not have occurred during a rain because the solution would have washed away and the features seen in Figure 2 obliterated. Instead, it is proposed that the thin layer of water which remains after a rainfall precipitation event absorbs acidic gases from the air before the surface dries and results in an acid electrolyte that dissolves rust. Then, on drying the dissolved material precipitates in the "valleys" and at the edge of the "reef-like" structures to gradually fill in the "valley" areas and level the corrosion film. The numerous small mounds in the valleys appear to be precipitate nucleation sites. The sites are fewer and larger at the rim of the solution filled areas, indicating a lower rate of precipitation when the solution volume is larger. But, as electrolyte evaporates and the solution draws down into the valley, the rate of precipitate nucleation increases and numerous small mounds consistent with accelerated drying are formed.

Cracks from an earlier drying cycle would not survive such extensive alteration of the surface. This evidently accounts for the absence of healed or partially healed cracks in the surface. The cracks apparently form as the last step in the drying cycle. New cracks, of course, can form along the path of earlier cracks.

The overall leveling that occurs in longer exposures suggests that the crests of the mounds are the most active sites for dissolution when wet. The water layer is thinnest here, and exchange with acidic gases from the atmosphere to produce a solution which will dissolve the rust should occur most rapidly at such sites. If the crests are sites of most active dissolution, then the "valleys" are the sites of most active precipitation and one follows the other as the volume of water retained on the surface decreases during drying. Horton (25) has observed that dust particles are found exclusively in the outer layer of the corrosion film. This is consistent with the massive reorganization of the film proposed here by a cycle of dissolution and precipitation during the latter stages of drying. The outer layer then corresponds to a solution altered structure modified intimately by contact with the environment, while the inner layer is modified basically by diffusion and conduction processes and is relatively isolated, except along crack lines, to massive intrusions of water.

In a few cases precipitation of material along cracks was observed, Figure 3. This was more likely to be seen on the groundward side than the skyward side, more often for exposures at the North Carolina site than New Jersey, and in longer exposures than in short exposures. The precipitated material is seen in Figure 3B to be densest along that portion of the crack lying in the depressions above and below the rim in the center of this figure. This is consistent with the observation that the higher areas of the film are sites of dissolution and the lower areas are sites for preciptation. Evidently, in the case shown in Figure 3, dissolved material from within the crack has moved to the surface where it precipitated as the corrosion film dried. Further drying then reformed the crack.

The three features described here suggest that the outer part of the corrosion films on carbon steel and Cor-Ten A undergo massive reorganization by a mechanism of solution and precipitation during the latter stages of drying. In many ways this process is similar for both materials and only differs in small but significant details related to the presence of alloying elements in the weathering steel. The ability to heal and self-repair the corrosion film is an essential aspect of forming a more protective corrosion film and would appear linked not only to the chemistry of the alloy but also to the chemistry of the interacting environment.

191 Zinc. In contrast to the steels, zinc does not yield a simple linear relationship between the amount of corrosion film retained on the surface and the zinc loss due to corrosion, Figure 4. The data fans out considerably with increasing weight loss. A mass balance on the 1-and 3-month data which define an upper limit to the amount of corrosion film retained on the surface, using Equation 6, yields a line with a slope b = 1.645. The small confidence interval for b, Table III, and the large number of points (N = 280) used in computing b would suggest that runoff and spalling of the zinc corrosion film are not a significant factor in the short-term exposures and that b is a consequence only of Equations 1 and 2. Values of b computed for the individual sites agree well with that shown in Figure 4 except for the District of Columbia site, where b = 1.41. Comparison of b with the theoretical values for various compounds, Table III, suggests that the corrosion film at the North Carolina, New Jersey, and New York sites is largely a combination of $Zn(OH)_2$ and $ZnCO_3$. Applying Equation 7 for a film composed of two main constituents, the difference between the experimental slope 1.645 and the theoretical slopes, 1.52 for $Zn(OH)_2$ and 1.92 for $ZnCO_3$, indicates a film consisting of about 30 wt pct $ZnCO_3$ and 70 wt pct $Zn(OH)_2$ in short-term exposures. The lower slope for the District of Columbia site strongly indicates the presence of ZnO. Slopes were also computed from Equation 8 using the results from the wet chemical analyses of the stripping solutions. The results agree with those from gravimetric determinations and lead to the same set of major constituents for the corrosion film, Table III. The computed slopes were, however, somewhat higher, as would be expected if there were some runoff losses, and recomputation of the corrosion film composition based on these slopes gave values nearer to 65 wt pct $ZnCO_3$ and 35 wt pct $Zn(OH)_2$ for short-term exposures at the North Carolina, New Jersey, and New York sites.

Corrosion film constituents identified by TGA in an inert atmosphere, Table IV, agree well with those determined by the mass balance on the corrosion film. Corrosion films on samples exposed at the District of Columbia and North Carolina sites for 1 to 12 months gave similar results. Pure $ZnCO_3$ was run as a standard. The large weight loss at 200°-250° C coincided exactly with the decomposition of $ZnCO_3$ and results reported by Anderson (26). Mass balance calculations indicate that the weight loss corresponds to between 40 and 100 wt pct $ZnCO_3$. No weight loss of the $ZnCO_3$ standard was observed below 200° C. Therefore, a small loss of weight from the corrosion film that occurs in the range 110°-200° C was interpreted as $Zn(OH)_2$ decomposition. X-ray diffraction spectra from the

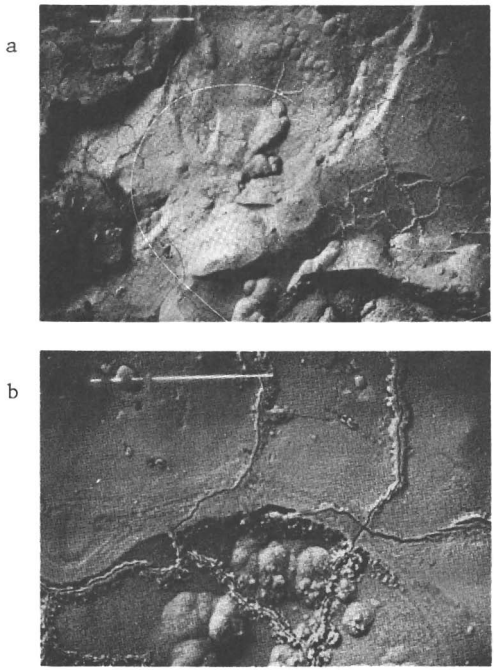

Figure 3. Groundward side of 1010 carbon steel microsample A46 exposed 3 years at NC site showing dissolution and precipitation features. Magnifications: (a) 80X; (b) 240X.

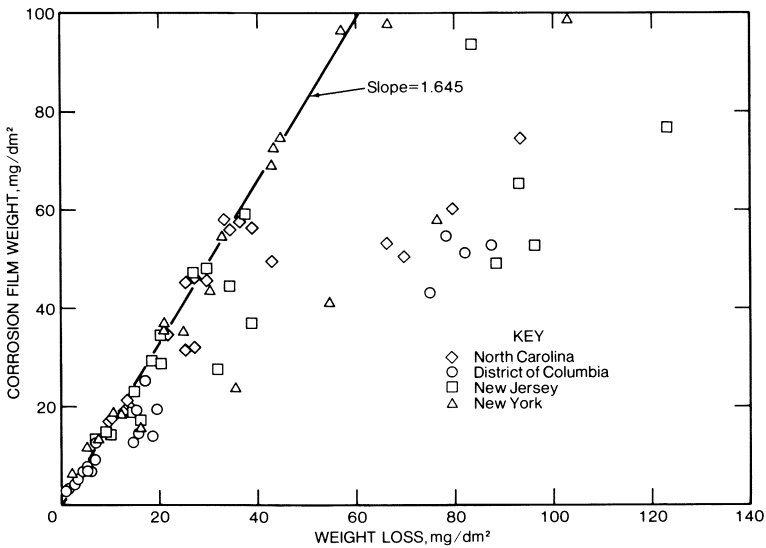

Figure 4. Mass of corrosion product retained on 191 zinc weight-loss panels in exposures of 1, 3, and 12 months at 4 sites. Exposures were initiated in period May 1982 - May 1983.

corrosion film on samples exposed for 3 years, Table V, contained several peaks which could not be matched with known phases. X-ray diffraction of the samples following TGA showed the corrosion film to be ZnO, the normal thermal decomposition product of $Zn(OH)_2$ and $ZnCO_3$.

Ion scattering spectroscopy of the corrosion film formed in 1-month exposures at the New York site gave an O/Zn atomic ratio consistent with ZnO in the outer 15 nm of the surface and which trended towards $ZnCO_3$ or $Zn(OH)_2$ deeper into the film, Table VII. The very outer 1 nm was rich in the surface contaminants Cl or S. Some Zn enrichment of the outer 15 nm of the film is observed which could be associated with the surface contaminants or related to drying effects.

Although many of the data points in Figure 4 lie on the mass balance line defined by the short-term data, a significant number of 3- and 12-month points lie in the fan-shaped area to the right of the line. Given the chemistry of long-term zinc corrosion products in the atmosphere (27), this shift cannot be due to the transformation of short-term corrosion products by weathering into some lower molecular weight compound. Instead, it represents a substantial loss of zinc corrosion product from the surface in runoff or possibly by spalling. SEM examination of the corrosion film on zinc samples exposed up to 36 months showed no evidence of spalling and, hence, it is assumed that this material loss is due entirely to runoff. The vertical difference between the data points in Figure 4 and the mass balance line roughly approximates the amount of this loss. However, a better estimate of the zinc loss to the environment in runoff is given by the difference in the gravimetric zinc weight loss and the zinc retained in the corrosion film as determined from the wet chemical analyses, i.e., $(m_A-R_L-S_L)$. This quantity is plotted in Figure 5 for 1-month exposures and in Figure 6 for 3- and 12-month exposures as a function of the total hydrogen ion load during the exposure period. The 1-month data in Figure 5 show that little, if any, of the corrosion film is lost in runoff due to hydrogen ion load or through dissolution in water. The zinc losses exhibit a roughly normal distribution about zero, and the wide distribution in values, particularly the negative values, are due to low precision in the wet chemical analysis of the corrosion film chemistry. This observation, that essentially no runoff losses occur in short-term exposures, is consistent with the earlier interpretation of the mass balance results for corrosion films formed in 1- and, in some cases, 3-month exposures.

The zinc losses for longer exposures, Figure 6, show a decidedly different result. Here there is an increasing trend of zinc loss from the corrosion film as the hydrogen ion load increases. A least squares fit of the data yields the following relationship between the zinc runoff loss, R_L(in mg Zn/dm^2), and the hydrogen ion load, x (mg H^+/m^2):

$$R_L = 0.746\ x \tag{11}$$

Assume, for simplicity, that the corrosion film is $ZnCO_3$ and that hydrogen ion reacts with the corrosion film to form bicarbonate. Equation 9 then becomes

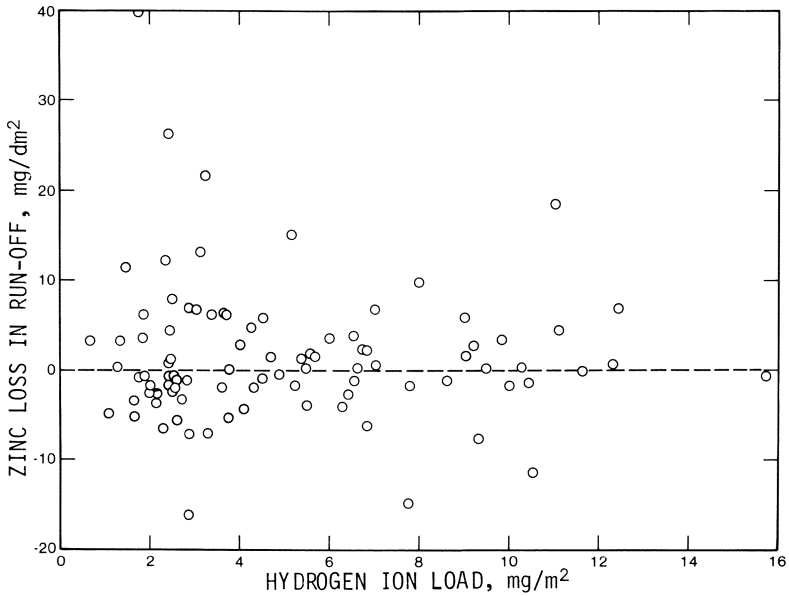

Figure 5. Influence of hydrogen ion loading on the dissolution of corrosion product during one-month exposures of 191 zinc at 4 sites.

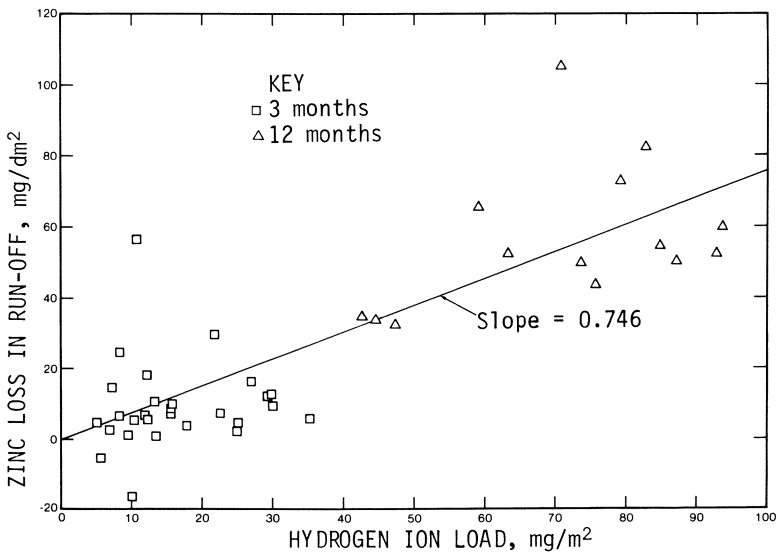

Figure 6. Influence of hydrogen ion loading on the dissolution of corrosion product during 3- and 12-month exposures of 191 zinc at 4 sites.

$$ZnCO_3 + H^+ \rightarrow Zn^{2+} + HCO_3^- \quad (12)$$

Using the annual average pH and the hydrogen ion load to estimate rainfall volume

$$y = \frac{(10^{-3+pH})X}{M_H} \quad (13)$$

Equation 10 can then be rewritten in form of Equation 11 to give

$$R_L = 0.0043 \left[fS_{ZnCO_3} \, 10^{-3+pH} \left(\frac{M_{Zn}}{M_{ZnCO_3}}\right) + M_{Zn} \right] \frac{X}{M_H} \quad (14)$$

The solubility of $ZnCO_3$ in neutral water is given as 10 mg/L (28). (The often quoted value given by Ageno and Valla (29), 206 mg/L, is evidently in error by a factor of 10 since they also report their value as 1.64×10^{-4} mole/L.) Substituting into Equation 14, using 4.2 as a reasonable annual average pH for the sites (6), and assuming that the runoff from the sample is saturated with $ZnCO_3$, i.e., f=1 gives

$$\begin{aligned} R_L &= (0.356 + 0.281)X \\ &= 0.637X \end{aligned} \quad (15)$$

This is in good agreement with Equation 11 and indicates that runoff losses from zinc are due to a combination of dissolution of corrosion product in water, the principal effect, and hydrogen ion loading. Equilibria involving CO_2, H_2CO_3, carbonate, and bicarbonate are also involved in the dissolution reaction and rough calculations have indicated that the runoff will be decidedly more basic than the incident rain. However, this does not alter the fact that hydrogen ion load is a significant factor in the dissolution of the zinc corrosion product.

Zinc corrosion rates decrease substantially with exposure time, Table I, indicating that the corrosion film is becoming increasingly more protective and retarding further corrosion. Moreover, corrosion rates at the four sites are converging to similar values even though there was a 6-fold difference in their initial rates. Thus, it would appear that a certain mass of corrosion product must form on the metal surface to provide the degree of protection observed in longer exposures. If runoff losses are significant, as suggested by Figure 6 and Equation 11, then zinc must corrode at a rate sufficient to replace the corrosion product lost by dissolution in long exposure times when roughly steady state conditions exist. In this way hydrogen ion load and acid deposition have a very specific and definable role in accelerating the corrosion of zinc.

Scanning electron microscopic examinations of zinc samples exposed 1, 12, and 36 months showed extensive reorganization of the corrosion film through repeated cycles of dissolution and precipitation not unlike that which occurs on carbon steel and Cor-Ten A. The corrosion product on zinc exposed 3 years at the New Jersey site, where short-term zinc corrosion rates are low, is uniform, somewhat nodular, and fine grained on both the skyward and groundward sites, Figure 7. The same was true for samples from the District of Columbia site. On the other hand, the corrosion film on

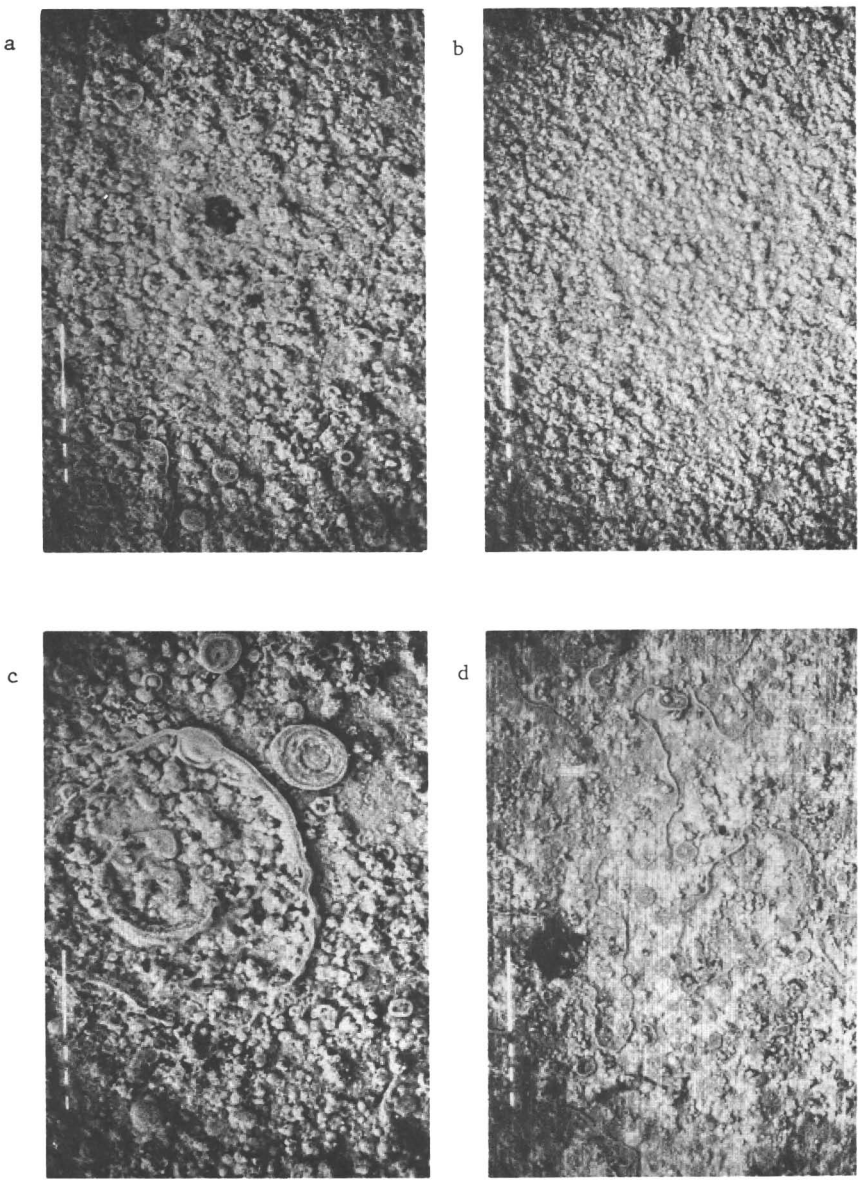

Figure 7. Microsamples of zinc 191 exposed 3 years. (a) skyward side and (b) groundward side, sample C43, from NJ site; (c) skyward side and (d) groundward side, sample C31, from NC site. Magnification: 136X.

zinc exposed 3 years at the North Carolina site, where short-term corrosion rates were highest, was very different from those for New Jersey and skyward and groundward sites were dissimilar. Massive dissolution and precipitation features are superimposed on the skyward side over a uniform, nodular corrosion product similar to that observed at New Jersey. These features, the enlarged and filled oval shapes and the curving solid barrier crossing dozens of the smaller nodular shapes, are evidence for a process of dissolution, concentration, redistribution, and precipitation that builds larger structures on the metal surface. Were this to happen during rainfall the dissolved material would wash away. Instead, as for the steels, it would appear to happen when the surface is drying and involves absorption of acidic gases from the atmosphere. The groundward side, Figure 7D, shows broad open areas covered by only a thin, porous corrosion product and bound by looping barriers of precipitated material. It would appear that corrosion on the groundward side of zinc exposed at the North Carolina site is substantially less than on the skyward side. Single-sided experiments are now in progress to confirm this possibility (6).

Figure 8 shows in greater detail the corrosion product that forms on the skyward side of zinc exposed at the North Carolina and New Jersey sites for 1 and 3 years. The massive features that develop at North Carolina in 3 years, Figure 8B, are not yet apparent after 1 year and the corrosion product that uniformly covers the surface, and on which is superimposed the nodular shapes, appears porous, Figure 8A. In contrast, the uniform layer covering the surface at New Jersey after 1 year, while cracked, is dense and shows evidence of dissolution and redistribution of material to give a corrosion film of more uniform thickness, Figure 8C. The corrosion product formed in 3 years exhibits several types of structures due to still unidentified phases, Figure 8D.

The SEM photomicrographs in Figures 7 and 8 show that reorganization of the zinc corrosion product on weathering is a complex phenomena involving competing processes. For the highly structured features to develop and be preserved over long periods, it is clear that, while dissolution does occur, the corrosion products are not readily soluble and accumulate rather than wash from the surface.

Galvanized Steel. The relationship between corrosion film weight and zinc weight loss for galvanized steel was similar to that shown in Figure 4 for zinc. There were, however, fewer points defining the line for the upper limit to the amount of corrosion product retained on the surface. There was also much more scatter in the data below this line indicating that substantial corrosion product was lost in runoff. The slope for the limiting line was 1.178, which would indicate that ZnO was a major constituent of the corrosion film. However, the slope was recomputed using the zinc present in the corrosion film as determined by wet chemical analysis of the film stripping solution, Equation 8. This produced a linear relationship with very little scatter between film weight and zinc in the corrosion film. Slopes computed from this data for each of the sites, including the Washington, DC, site, were in good agreement and ranged from 1.45 to 1.55. These values are consistent with a corrosion film containing $ZnCO_3$, ZnO, and $Zn(OH)_2$, as reported by

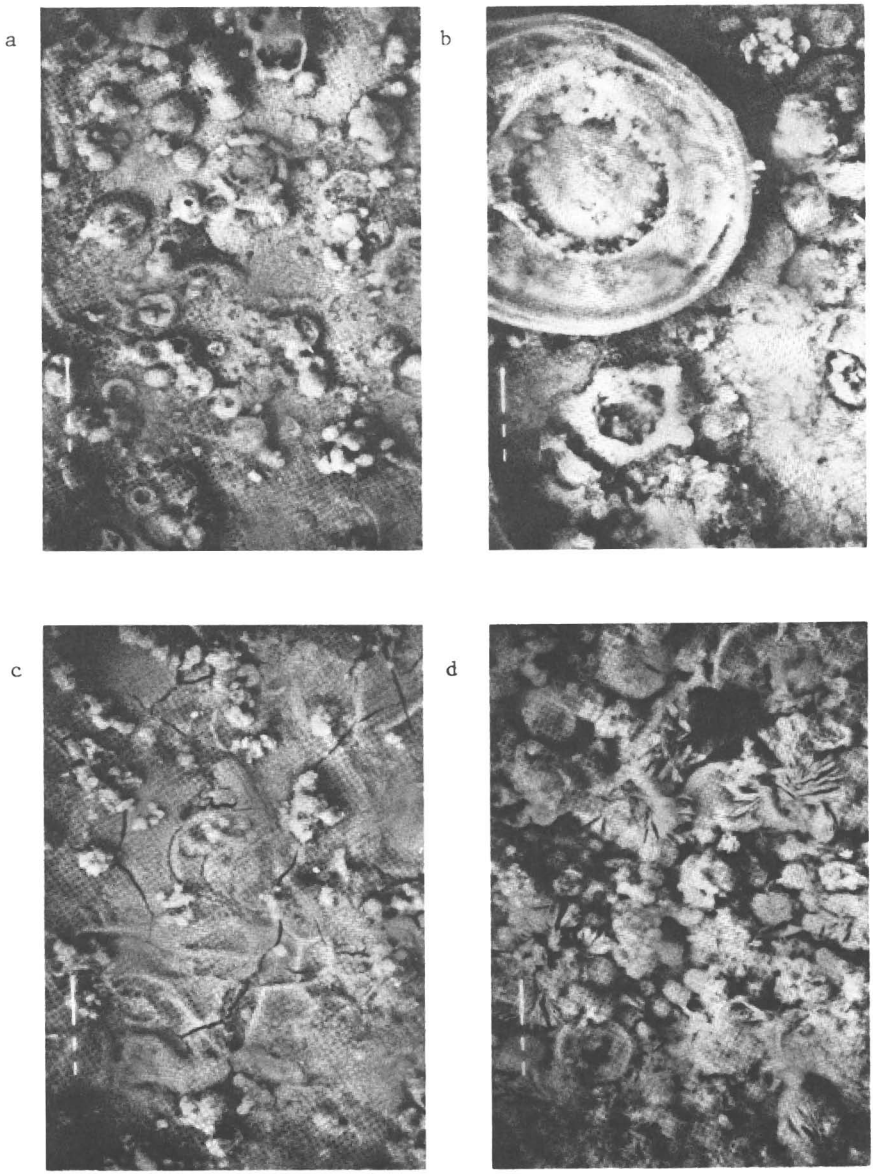

Figure 8. Skyward side of 191 zinc microsamples. (a) 1-year exposure and (b) 3-year exposure at NJ site; (c) 1-year and (d) 3-year exposure at NC site. Samples are (a) C229; (b) C31; (c) C231; (d) C43. Magnification: 720X.

Biestek (27) and Barton (30). Assuming a 2-constituent corrosion film of $ZnCO_3$ and ZnO, a slope of 1.5 corresponds roughly to a corrosion film consisting of 60 wt pct $ZnCO_3$ and 40 wt pct ZnO.

The slopes and the constituents associated with those slopes are different for zinc and galvanized steel. This was unexpected since, to the atmosphere, they should appear the same. However, there was one significant difference between the two materials. The surface of the galvanized steel received a chromate treatment to improve its resistance to "white rusting" during storage (31, 32).

X-ray photoelectron spectroscopy, and ISS analysis of the corrosion film on galvanized steel has shown that the surface is rich in chromium from this chromate treatment, Tables VI and VII. XPS analysis shows both Cr^{3+} and Cr^{6+} present in the corrosion film following a 1-month exposure at the New York site; Cr^{3+} was as much as 6 times more abundant in the corrosion film than Cr^{6+}. Lead was a minor constituent of the corrosion film, probably as PbO or Pb_3O_4. Three peaks were found for oxygen; a relatively small one for the chromium oxides; one for $ZnCO_3$; and a third identified as $Zn(OH)_2$. ISS shows as much as 13 at pct Cr in the outer 1 nm of the corrosion films and small amounts of aluminum. Beyond 1 nm into the corrosion film, the oxygen concentration, after correcting for the amount combined with Cr in Cr_2O_3 and Al in Al_2O_3, was stoichiometrically equivalent to ZnO. The corrosion film on galvanized steel may be similar to that on zinc where there appears to be a ZnO layer on the outer surface, perhaps as a consequence of drying, and $Zn(OH)_2$ is a constituent deeper into the corrosion film. These results clearly show that Cr is present in substantial amounts on the surface of the galvanized steel corrosion film and evidently serves to inhibit the corrosion of the zinc coating.

SEM examination of galvanized steel exposed 3 years at the North Carolina site shows very different corrosion films on the groundward and skyward sites, Figure 9. The large solution-altered features on the skyward side look not unlike those for zinc exposed at the same site. However, the small nodular structure observed on zinc was not present in the corrosion film on galvanized steel and there were areas (one appears as a smooth white area in the lower right corner of Figure 9A) which are uncorroded. These areas are presumed to be due to the continued passivation of the surface by the residual chromate coating. The groundward side, Figure 9B, is characterized by large areas of uncorroded surface. Small areas of localized breakdown are distributed over this surface including areas where corrosion has proceeded along scratch marks. It is probable that these scratches occurred after the chromate treatment and penetrate the protective chromate layer. By removing the chromate in these areas the scratches have made the zinc coating more susceptible to corrosion.

Given the nonuniform distribution of corrosion on the surface of the galvanized steel it is possible that the ISS and XPS results concerning ZnO and $Zn(OH)_2$ are not in conflict; two distinctly different areas may have been examined. Perhaps a largely uncorroded surface, as seen in Figure 9B, was examined by ISS. This area would then be characterized as passivated by Cr and consisting of a thin ZnO layer. On the other hand, corrosion product from a more actively corroding surface, as in Figure 9A, may have been examined by

XPS. This area would be characterized as containing substantial water and $Zn(OH)_2$ and $ZnCO_3$ as well as ZnO.

Three-year corrosion films on galvanized steel from the New Jersey site did not possess solution-altered features on the skyward side. This was true also for the corresponding zinc samples. There were, however, substantial areas of uncorroded surface on both the skyward and groundward sides. While short-term corrosion rates are different between zinc and galvanized steel, in long-term exposures there are close parallels in the development of the weathered corrosion film on both materials.

Galvalume. A plot of film weight versus weight loss showed a scatter of points with a poorly defined upper limit like that for galvanized steel. Corrosion film weights were often less than the weight of material which had dissolved to form the corrosion film. This indicates that Galvalume, like the other zinc containing materials, loses corrosion product to runoff during exposure.

SEM photomicrographs of an unexposed Galvalume blank and Galvalume exposed 3 years at the New Jersey site are shown in Figure 10. Galvalume is a 2-phase AlZn coating which consists of an Al-rich dendritic phase and a Zn-rich interdendritic phase (33). These structures are clearly evident in Figure 10A for the blank, with most of the surface covered by the oxide on the Al-rich phase, and with isolated windows through this dendritic phase exposing the Zn-rich phase. Corrosion appears to be confined largely to those areas where the Zn-rich phase is exposed, Figure 10B. Average corrosion rates were less than 1 μm/y in 1-month exposures at the New Jersey site from May 1982 through May 1984 (6). Actual corrosion rates would be substantially higher than this if based on the area that is corroding, i.e., the interdendritic phase. The voids that are produced in this area leave a surface which, on a microscopic scale, is quite rough and can readily trap fine dust particles, aerosols, and corrosion product.

110 Copper. Plots of film weight versus metal loss for 1- and 3-month exposures of 110 copper generally show a linear relationship between film weight and metal loss. If 1-year exposures are included in the plot they will be scattered and fall below the line established by the 1- and 3-month exposures. This may be an indication of runoff losses in longer exposures. The lines based on short-term data had slopes of 1.12, 1.19, 1.10, and 1.08 for the North Carolina, New Jersey, New York, and District of Columbia sites, respectively, when based on gravimetric data, Equation 6. The District of Columbia data points exhibited somewhat greater scatter then the other sites, which could represent increased runoff loss for these samples.

Plots of film weight versus the copper determined by wet chemistry from the stripping solutions, Equation 8, are linear. The slopes--1.12, 1.15, 1.14, and 1.20 for the North Carolina, New Jersey, New York, and District of Columbia sites--generally confirm the results from the gravimetric data. No significant site-to-site differences were apparent in the slopes. The District of Columbia site had a slightly higher slope using the wet chemical analyses, but it also had the lowest slope by gravimetric methods. The slopes fell between the theoretical values for pure CuO and Cu_2O,

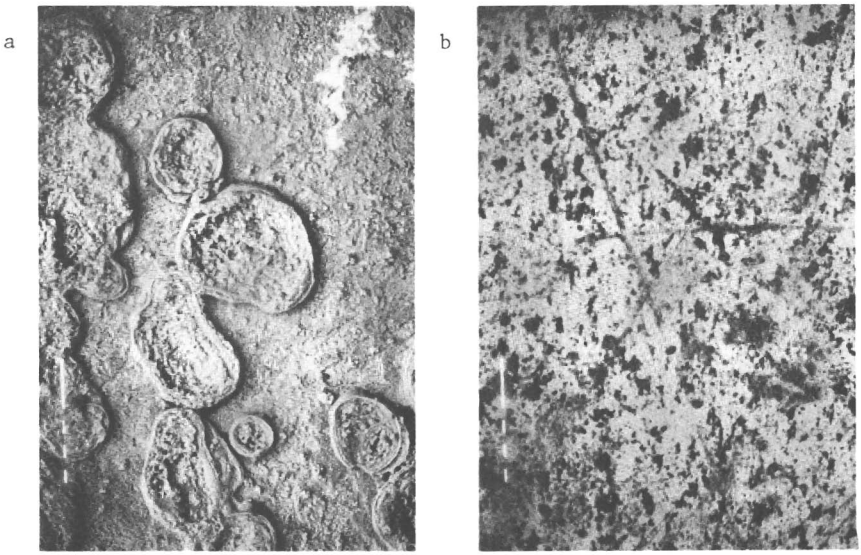

Figure 9. Skyward (a) and groundward (b) sides of galvanized steel microsample G51 exposed 3 years at NC site. Magnification: 80X.

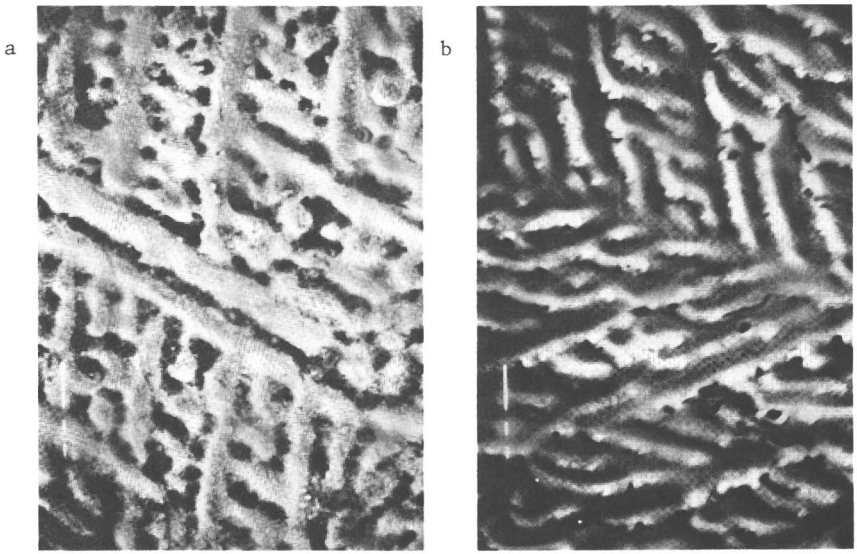

Figure 10. Galvalume blank (a) and skyward side of microsample F38 (b) exposed 3 years at NJ site. Magnification: 720X.

Table III, indicating that the film is composed primarily of these two constituents. These results are consistent with observations of Mattson (34), who indicated that Cu_2O was the primary film constituent for short-term exposures.

ISS analysis of copper films confirmed that the film is composed mostly of oxygen and copper. The atomic percentage of chlorine or sulfur is relatively small and diminishes rapidly with distance into the film. Thermal analysis results for 1-month and 1-year exposures, Table IV, rule out the possibility that large amounts of sulfur, chlorine, or carbonate containing compounds are present in the film. A slow, constant rate of weight loss was observed at temperatures between 110° and 350° C by TGA which was not typical of the thermal decomposition reported for any inorganic copper compounds (23). In measurements on pure CuO, no weight change was observed in this temperature range. Interaction of carbonaceous material deposited on the film with CuO to produce Cu_2O and CO_2 could possibly explain the slow weight loss from samples during TGA. X-ray diffraction results, Table V, show the presence of Cu_2O in samples both before and after TGA.

The SEM photomicrographs in Figure 11 show that copper corrodes locally and nonuniformly. Figure 11B shows a sample, exposed for 1 year at the North Carolina site, which has had its corrosion film stripped. Flat uncorroded areas, identified by the rolling marks from the original copper surface, are present. Figure 11A shows a similar sample with the corrosion film intact. Thick mounds formed in the corrosion film appear to be associated with the areas of localized metal attack seen in Figure 11B.

XPS was used to study films on copper samples from several sites for different exposure periods. As indicated in Table VIII major changes in the composition of the corrosion film surface appear to be occurring with time. Different sites gave similar results for the same exposure period, although there was some variation in the $ClS_{1/2}$ peaks among the sites. This could indicate that the nature of the carbon compounds being deposited on the film varies from site to site. The $Cu2P_{3/2}$ peak was interpreted using data from Schon (35) to distinguish CuO from Cu and Cu_2O. It was not possible to separate the contributions of Cu and Cu_2O. The 1-month samples showed large amounts of both CuO and Cu or Cu_2O. At longer exposures the amount of CuO increased while the amount of the less oxidized species decreased. The groundward sides of the samples tended to have less CuO and more Cu_2O or Cu than the skyward. The results indicate that a layer of CuO is produced in the outer 10 nm of the film surface with increasing exposure time and that this process proceeds faster on the skyward side than the groundward side.

3003-H14 Aluminum. The Al-Mn 3003 alloy corrodes at rates less than 0.1 μm/y in exposures of 1, 3, and 12 months. Rates at the New Jersey site are 2 to 3 times those at the other sites. SEM examination showed pitting in exposures of 12 and 36 months, Figure 12. The pits were in the early stages of development with a small, deeper central area surrounded by shallow localized attack radiating outwards, particularly along grain boundaries. This type of attack is similar to that described by Sowinski (36). Pits were more fully developed at the New Jersey site, encompassing a larger area of

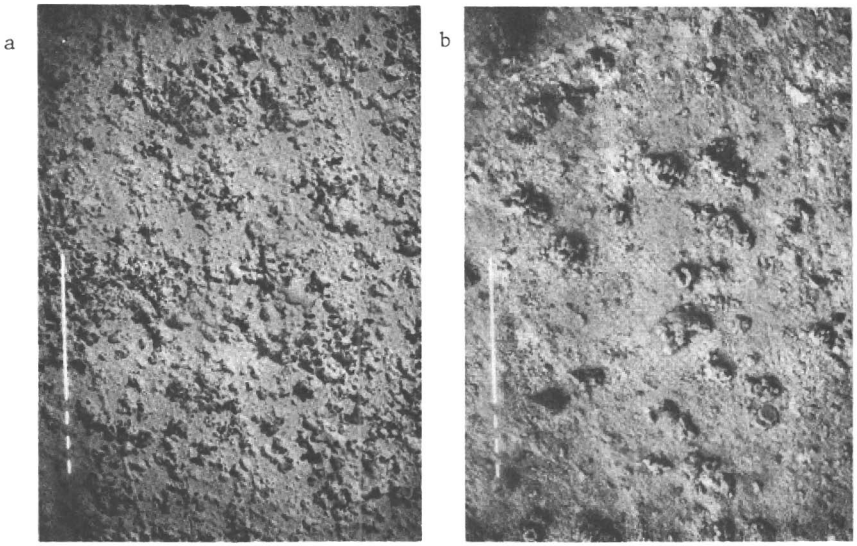

Figure 11. Skyward side of 110 copper exposed 1 year at NC site. (a) microsample D231 with corrosion film intact; (b) wieght-loss panel D1-91 after removing corrosion film. Magnification: 240X.

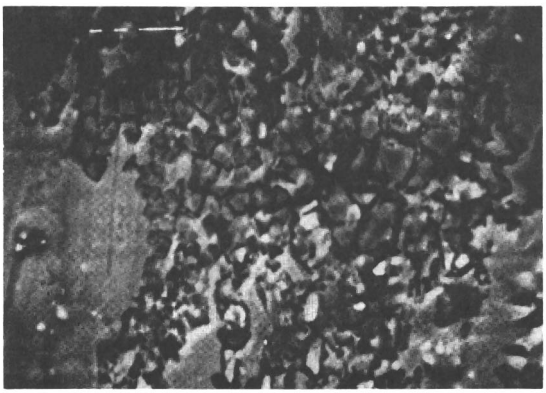

Figure 12. Skyward side of aluminum 3003-H14 weight-loss panel B2-73 exposed 1 year at NJ site after removing corrosion film. Magnification: 720X.

Table VIII. X-ray photoelectron spectroscopic analysis of corrosion film on microanalysis samples

Metal/Exposure	XPS Peak	Observation[1]
110 Copper/1 month	$Cu2P_{3/2}$	Cu, Cu_2O: major CuO: major Less Cu as CuO on groundward side than skyward side.
	$C1S_{1/2}$	C-H, C-C: major C-O, C=O: minor
	$O1S_{1/2}$	Oxide [CuO, Cu_2O]: major hydroxide, water: minor C=O, C-O: minor
110 Copper/1 year	$Cu2P_{3/2}$	Cu, Cu_2O: major CuO: major CuO > Cu, Cu_2O
	$C1S_{1/2}$	C=O, C-O: major C-H, C-C: minor
110 Copper/3 year	$CuIP_{3/2}$	skyward side-CuO: major groundward side-CuO: major Cu, Cu_2O: minor
	$C1S_{1/2}$	C=O, C-O: major C-H, C-C: minor
	$O1S_{1/2}$	C=O, C-O: major oxide [CuO, Cu_2O]: minor

[1]Phases in brackets indicate probable identities of peaks.

American Chemical
Society Library
1155 16th St. N. W.
Washington, D. C. 20036

localized breakdown and involving more intense dissolution of grains and grain boundaries. Pitting was more evident on the skyward side than the groundward side of the samples. Also present on the skyward side was a finely structured nonuniform general attack which textured the surface in exposures of 3 years and obscured original surface detail such as rolling marks and fine scratches. This attack may be associated with small intermetallic $FeAl_3$ and $FeMnAl_6$ precipitates dispersed in the 3003 alloy. Similar texturing of the groundward side had not occurred in 3-year exposures and much of the surface detail was retained.

Conclusions

For purposes of analysis, growth of an atmospheric corrosion film was viewed schematically as a three step process consisting of: (1) formation of a corrosion product; (2) weathering of that product while conserving mass of the metal; and (3) corrosion product losses through runoff and spalling. One or more of these steps may be occurring during any stage in film growth depending upon the material and the environment. Corrosion films formed on metals and metal-coated steel products exposed by the Bureau of Mines at field sites in the eastern U.S. for times from 1 to 36 months had: (1) chemistries that were independent of environment in short-term exposures; (2) morphologies that were, in some cases, highly altered by solution processes; and (3) runoff losses for zinc that were dependent upon hydrogen ion loading.

Corrosion Film Chemistry. A linear relationship exists between the mass of corrosion product formed on carbon steel, Cor-Ten A, zinc, galvanized steel, and copper and the mass of metal in the corrosion film. This relationship is independent of site and the wide variation in environmental parameters between the sites in short-term exposures of 1 and 3 months. The ratio of the two masses is relatively sensitive to the composition of the corrosion film. The independence of this ratio from substantial variations in air quality, meteorology, and rain chemistry is interpreted as indicating, at least for the major constituents, that the composition of the corrosion film is independent of the environment in short-term exposures.

The corrosion film on Cor-Ten A contains between 30 and 70 wt pct FeOOH, about 4-12 wt pct loosely-bound water, about 1-5 wt pct water of hydration, and the balance hydrated Fe_2O_3. No significant concentrations of FeO, Fe_2O_3, Fe_3O_4, $FeSO_4$, and $Fe(OH)_2$ are present. The corrosion film on carbon steel is similar to that on Cor-Ten A in short exposures.

The corrosion film on zinc contains about 65 wt pct $ZnCO_3$ and 35 wt pct $Zn(OH)_2$. The corrosion film from the Washington, DC, site may also contain ZnO. The corrosion film on galvanized steel consists of $ZnCO_3$, $Zn(OH)_2$, and ZnO. The presence of the ZnO is probably due to the stabilization of an initial passive ZnO film by Cr^{3+} which persists over parts of the surface in exposures up to 3 years.

The corrosion film on copper contains mostly Cu_2O and some CuO. The corrosion films from the Washington, DC, site contain a higher percentage of CuO, i.e., 40 wt pct Cu_2O and 60 wt pct CuO. The

films do not contain large amounts of the copper sulfides, sulfates, hydroxides, carbonates, chlorides, or combinations of these compounds.

Corrosion Film Weathering. Significant spalling and runoff losses occur for all of the metals in exposures of 1 year. Zinc and galvanized steel exhibit runoff losses in 3- and 12-month exposures. Massive reorganization of the corrosion films on carbon steel, Cor-Ten A, zinc, and galvanized steel occurs which produces new morphologies in the weathered film. These morphologies are dependent on site, exposure time, and orientation (skyward and groundward). They develop over extended periods of time, indicating that the solution and precipitation processes producing them do not occur primarily during precipitation events, when washing would totally remove dissolved corrosion products, but during the drying phase of precipitation events and when moisture collects on the surface with little or no runoff, as with dew. The solution present on the surface during the drying phase is a powerful solvent, altering features of the corrosion film which appear unaffected by the continuous washing of rain. Absorption of acidic gases from the atmosphere is probably important to the formation of this solvent. With continuing evaporation of the solution, dissolution of corrosion product diminishes and precipitation begins. Differences exist in the details of this process for the individual metals, e.g., Cor-Ten A and zinc. Corrosion rates for all of the metals except Galvalume and aluminum decrease with increasing time, indicating the formation of a more protective corrosion film in the longer exposures. Conditions which affect the weathering processes described here will have a marked effect on the corrosion of the metals themselves, as their ability to achieve a stable, low corrosion rate in long-term exposures depends entirely on the development of the corrosion film.

Runoff Losses Due to Hydrogen Ion Loading. Runoff losses from zinc, and presumably galvanized steel, are dependent upon hydrogen ion load in 3- and 12-month exposure. Such an effect is not apparent in 1-month exposures. Hydrogen ion dissolves zinc carbonate, perhaps the major constituent of the corrosion film, by the reaction

$$ZnCO_3 + H^+ \rightarrow Zn^{2+} + HCO_3^-$$

Additional corrosion film is lost in the runoff due to the limited solubility of the corrosion product in rain. The relative contribution of these effects to the runoff in 3- and 12-month exposures was 55 pct dissolution and 45 pct hydrogen ion loading. To maintain the stable corrosion film that develops on zinc in long-term exposures, it is evident that zinc must corrode at a rate sufficient to replace the corrosion product lost in runoff.

Acknowledgment

This research has been funded by the Bureau of Mines and the National Acid Precipitation Assessment Program through a cost-sharing Interagency Agreement between the Bureau and the Environmental Protection Agency. Use of trade names or company names does not imply endorsement by the Bureau of Mines.

Literature Cited

1. Flinn, D. R.; Cramer, S. D.; Carter, J. P.; Lee, P. K; Sherwood, S. I. "Acidic Deposition and the Corrosion and Deterioration of Materials in the Atmosphere: A Bibliography. 1880-1982"; PB83-126091; National Technical Information Service, July 1983.
2. Haynie, F. H.; Upham, J. B. In "Corrosion in Natural Environments"; STP 558; American Society for Testing and Materials: Philadelphia, 1974; 33-51.
3. Mansfeld, F. B. "Effects of Airborne Sulfur Pollutants on Materials"; PB81-126351; National Information Service, January 1980.
4. Lipfert, F. W.; Benarie, M.; Daum, M. L. Derivation of Metallic Corrosion Damage Functions For Use in Environmental Assessments. Draft Report, available from senior author, Dept. of Energy and Environment, Brookhaven National Laboratory, Upton, NY 11973.
5. Franey, J. P.; Graedel, T. E.; Kammlott, G. W. In "Atmospheric Corrosion"; Ailor, W. H., Ed.; John Wiley and Sons: New York, 1982; 383-392.
6. Flinn, D. R.; Cramer, S. D.; Carter, J. P.; Spence, J. W. Durability of Building Materials, 1985, 3(2), 147-175.
7. Bureau of Mines. Quality Assurance Project Plan. Interagency Agreement AD-14-F-1-452-0 between Bureau of Mines and Environmental Protection Agency, October 1983. (Available from D. R. Flinn, Bureau of Mines, Avondale Research Center, Avondale, MD 20782-3393.)
8. Reddy, M. M.; Sherwood, S. I. Limestone and Marble Dissolution by Acid Rain. In this book.
9. Youngdahl, C. A.; Doe, B. R.; Sherwood, S. I. Roughening Recession and Chemical Alteration of Marble and Limestone Sample Surfaces After Atmospheric Exposure in the Northeastern United States. In this book.
10. Cohen, M.; Hashimoto, K. J. Electrochem. Soc., 1974, 121(1), 42-45.
11. Inouye, K.; Ichimura, K.; Kaneko, K.; Ishikawa, T. Corrosion Sci., 1976, 16, 507-517.
12. Kameko, K.; Inouye, K. Bull. Chem. Soc. of Japan, 1976, 49(12), 3689-3690.
13. Suzuki, I.; Masuko, N.; Hisamatsu, Y. Corrosion Sci., 1979, 19, 521-535.
14. Cramer, S. D.; Carter, J. P.; Covino, B. S., Jr. "Atmospheric Corrosion Resistance of Steels Prepared from the Magnetic Fraction of Urban Refuse"; U.S. Bureau of Mines, RI 8477, 1980.
15. Suzuki, I.; Hisamatsu, Y.; Masuko, N. J. Electrochem. Soc., 1980, 127(10), 2210-2215.
16. Matijevic, E. Pure and Applied Chemistry, 1980, 52(5), 1179-1193.
17. Spedding, D. J.; Sprott, A. J. Proc. 8th Intern. Congr. Met. Corr.; Dechema: Frankfurt, 1981; Vol. 1, 329-335.
18. de Meybaum, B. R.; Ayllon, E. S.; Bonard, R. T.; Granesse, S. L.; Ikeha, J. L. Proc. 8th Intern. Congr. Met. Corr.; Dechema: Frankfurt, 1981; Vol. 1, 317-322.

19. Keiser, J. T.; Brown, C. W.; Heidersbach, R. H. Corrosion, 1982, 38(7), 357-360.
20. Leidheiser, H., Jr.; Czako-Nagy, I. Corrosion Sci., 1984, 24(7) 569-577.
21. Cleary, H. J. Corrosion, 1984, 40(11), 606-608.
22. Albrecht, P.; Naeemi, A. H. "Performance of Weathering Steel in Bridges"; National Cooperative Highway Research Program Report 272, Transportation Research Board, National Research Council: Washington, DC, 1984.
23. Liptay, G. "Atlas of Thermoanalytical Curves"; Heyden and Sons: New York, 1971; Vol. 2, Section 89.
24. Evans, U. R. "The Corrosion and Oxidation of Metals"; E. Arnold: London, 1960; p. 25.
25. Horton, J. B. Proc. San Francisco Regional Technical Meeting; American Iron and Steel Institute: Washington, DC, November 18, 1965; 171-195.
26. Anderson, E. A.; Fuller, M. L. Metals and Alloys, 1939; Vol. 10, pp. 292-287.
27. Biestek, T. In "Atmospheric Corrosion"; Ailor, W. H., Ed.; John Wiley and Sons: New York, 1982; 631-643.
28. Handbook of Chemistry and Physics; 60th Ed.; CRC Press: Boca Raton, FL, 1979; B-142.
29. Ageno, F.; Valla, E. Hydrolysis. Atti Accad. Lincei, 1911; Vol. 20, Part II, 706-712.
30. Barton, K. "Protection Against Atmospheric Corrosion"; Wiley and Sons: New York, 1973; 49.
31. Williams, L. F. G. Plating, 1971, 59(10), 931-938.
32. Duncan, J. R. Surface Technology, 1982, 16, 163-173.
33. Zoccola, J. C.; Townsend, H. E.; Borzillo, A. R.; Horton, J. B. In "Atmospheric Factors Affecting the Corrosion of Engineering Materials"; STP 646; Coburn, S. K., Ed.; American Society for Testing Materials: Philadelphia, 1978; 165-184.
34. Mattson, E.; Holm, R. In "Atmospheric Corrosion"; Ailor, W. H., Ed.; John Wiley and Sons: New York, 1982; 365-381.
35. Schon, G. Surface Sci., 1973, 35, 96-108.
36. Sowinski, G.; Sprowls, D. O. In "Atmospheric Corrosion"; Ailor, W. H., Ed.; John Wiley and Sons: New York, 1982; 297-328.

RECEIVED January 2, 1986